Santamaria-Perez, David; Gomis, Oscar; Sans, Juan Angel; et ál.. (2014). Compressibility systematics of calcite-type borates : An experimental and theoretical structural study on ABO3 (A = Al, Sc, Fe and In). Journal of Physical Chemistry C. 118:4354-4361. doi:10.1021/jp4124259.

COMPRESSIBILITY SYSTEMATICS OF CALCITE-TYPE BORATES: AN EXPERIMENTAL AND THEORETICAL STRUCTURAL STUDY ON ABO_3 (*A* = Al, Sc, Fe and In).

David Santamaría-Pérez[1*,♣], Oscar Gomis[2], Juan Angel Sans[3], Henry. M. Ortiz[3], Angel Vegas[4], Daniel Errandonea[1], Javier Ruiz-Fuertes[1], Domingo Martinez-Garcia[1], Braulio Garcia-Domene[1], André L.J. Pereira[3], Francisco Javier Manjón[3], Placida Rodríguez-Hernández[5], Alfonso Muñoz[5], Fabio Piccinelli[6], Marco Bettinelli[6], Catalin Popescu[7]

[1] Departamento de Física Aplicada-ICMUV, MALTA Consolider Team, Universidad de Valencia, C/Dr. Moliner 50, Burjassot, 46100 Valencia (Spain)

[2]Centro de Tecnologías Físicas: Acústica, Materiales y Astrofísica, MALTA Consolider Team, Universitat Politècnica de València, Camí de Vera s/n, 46022 València (Spain)

[3]Instituto de Diseño para la Fabricación y Producción Automatizada, MALTA Consolider Team, Universitat Politècnica de València, Camí de Vera s/n, 46022 València (Spain)

[4] Universidad de Burgos, Plaza Misael Bañuelos, 09001 Burgos (Spain)

[5]MALTA Consolider Team - Departamento de Física Fundamental II, Instituto Univ. de Materiales y Nanotecnología, Universidad de La Laguna, La Laguna, Tenerife (Spain)

[6]Laboratory of Solid State Chemistry, University of Verona, Strada Le Gracie 15, 37134 Verona (Italy)

[7]ALBA-CELLS, Carretera BP 1413, 08290 Cerdanyola, Barcelona (Spain)

KEYWORDS: Orthoborates, high-pressure, carbonates, compressibility systematics

ABSTRACT: The structural properties of calcite-type orthoborates ABO_3 (*A* = Al, Fe, Sc and In), have been investigated at high pressures up to 32 GPa. They were studied experimentally using synchrotron powder x-ray diffraction and theoretically by means of *ab initio* total-energy calculations. We found that the calcite-type structure remains stable up to the highest pressure explored in the four studied compounds. Experimental and calculated static geometries (unit-cell parameters and internal coordinates), bulk moduli and their pressure derivatives are in good agreement. The compressibility along the *c* axis is roughly three times that along the *a* axis. Our data clearly indicate that the compressibility of borates is dominated by that of the $[AO_6]$ octahedral group and depends on the size of the trivalent *A* cations. An analysis of the relationship between isomorphic borates and carbonates is also presented, which points to the potentiality of considering borates as chemical analogues of the carbonate mineral family.

1.- Introduction

$A^{III}BO_3$ metal orthoborates have been known for many years to be isostructural with different forms of calcium carbonate, $CaCO_3$. In particular, Al, Sc, Ti, V, Cr, Fe, In, Yb, and Lu borates crystallize in the calcite-type structure; Y, Sm, Eu, Gd, Dy ,Ho, Er, Tm, Yb, and Lu adopt the vaterite-type structure; and La, Ce, and Nd borates are found in the aragonite-type structure. Which polymorph is stable at room conditions can be explained in terms of the classical crystal radii ratio $r_{AO}= A^{3+}/O^{2-}$, being calcite if $r_{AO} < 0.8$, vaterite if $0.8 < r_{AO} < 0.89$ and aragonite if $r_{AO} > 0.89$ [1]. This hypothesis agrees roughly with the critical value in $CaCO_3$ ($r_{AO} \sim 0.9$) which is found in the three polymorphs [2]. These structural similarities are based on the stability of the $[BO_3]^{3-}$ and $[CO_3]^{2-}$ groups, where B and C bond to three oxygen atoms in triangular planar configuration [3]. In connection with this, infrared spectroscopy suggests a non-planar boron – oxygen configuration for vaterite-type borates [2], boron having tendency toward oxygen coordination greater than 3, which could also explain the instability of this structural type in carbonates. In spite of the greater stability of the borate anion group, mineral species of the borate class tend to occur rarely in geologic formations due to the small elemental abundance of B and A^{III} metals in Earth's interior [4]. Nevertheless, borates could be considered as analogues of carbonates and could help in demonstrating the effects of tuning the thermodynamic variables as well as the cation substitution in these types of structures.

The four borates considered in this manuscript: Aluminum [5], scandium [6], iron [7] and indium [8] orthoborates crystallize in the calcite-type structure (space group (S.G.): R-3c, No. 167, Z=6), which is the less dense of the afore-mentioned polymorphs. These compounds have a wide potential at room conditions for their application in photoluminescence. Rare-earth-doped ABO_3 emitting phosphors are known for fifty years [9]. $ScBO_3$, for instance, operates as a room-temperature near-infrared tunable laser when doped with Cr^{3+} [10] and $InBO_3$ doped with Eu^{3+} has been studied due to their properties as scintillating material [11]. Particularly interesting is iron borate $FeBO_3$, which is a weak antiferromagnet at ambient conditions [12].

The most important features of the calcite structure are depicted in **Figure 1a**. It is formally described as formed by slightly distorted $[A^{III}O_6]$ octahedra whose O atoms belong to different $[BO_3]$ units. The borate groups are distributed in layers in such a way that the triangular $[BO_3]$ groups present reversed orientations in alternating layers; while $[AO_6]$ octahedra share corners with other six octahedra, three from the upper layer and three from the lower layer. Structural analyses in terms of second-neighbour contacts have proven to be particularly useful in determining high pressure and temperature tendencies and polymorphism [13-16]. In this sense, the calcite structure can also be thought of as a distorted rocksalt structure of the *A* and B atoms (see **Fig. 1b**); where the primitive rhombohedral unit-cell of calcite can be obtained by compressing the cubic NaCl-like structure along the threefold symmetry axis [111] [17].

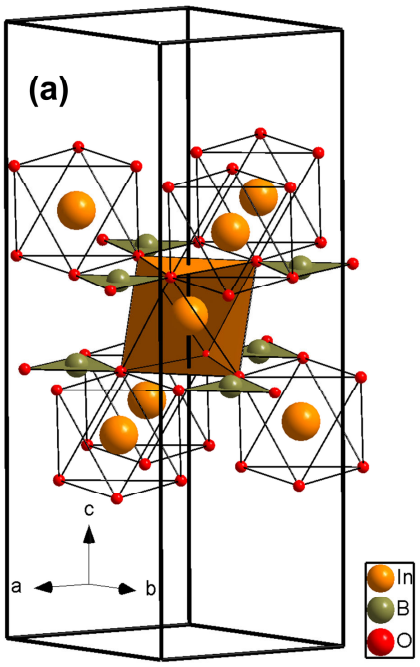

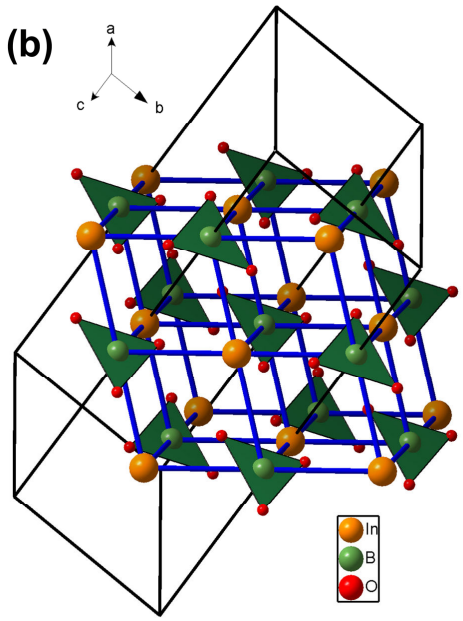

FIGURE 1: (a) Crystal structure of the rhombohedral R-3c calcite-type $InBO_3$. [BO_3] triangle units are depicted in green. An [InO_6] octahedron is represented in orange together with six additional [InO_6] octaedra with which it shares one corner. O atoms are represented in red. Cell edges are shown as solid black lines. (b) Distorted rocksalt structure of the InB subarray in $InBO_3$ (angle ∠B-In-B = 76.4º at room conditions). In, B, and O atoms are represented as orange, green and red spheres, respectively. The solid blue lines would indicate the B – In contacts.

In this paper we report a high pressure (HP) study of the rhombohedral calcite-type structure of aluminium, scandium, iron and indium borates from both theoretical and experimental points of view. Angle-dispersive powder x-ray diffraction (XRD) measurements were carried out at room temperature up to 32 GPa. Their equations of state and axial compressibilities have been determined. We will particularly focus on the special geometrical features occurring when pressure is applied. Finally, we will discuss the analogies between the behaviour of calcite-type borates and carbonates. The structural evolution of the second coordination sphere of cations with pressure will provide some hints on the nature of this class of compounds.

2.- Experimental and theoretical details

Synthesis.- **(i)** $AlBO_3$ single crystals were prepared by hydrothermal HP synthesis [18]. **(ii)** $FeBO_3$ crystals were obtained from a 1:1:5 Fe_2O_3:Bi_2O_3:B_2O_3 flux. After fusion at about 1200 ºC, the melt was annealed for several days [7,19]. **(iii)** $ScBO_3$ ($InBO_3$) single crystals were prepared by the flux growth method [20], where appropriate quantities of pure Sc_2O_3 (In_2O_3), B_2O_3 and $LiBO_2$ were used as starting materials. After careful mixing, the starting mixtures were heated to 1150 °C with a heating rate of 100°C h^{-1}. The melt was maintained at this temperature for 10 h (soaking time), then cooled to 840 °C at a rate of 3 °C h^{-1}. Finally, it was cooled down to room temperature at a rate of 100 °C h^{-1}.

Single crystal x-ray diffraction at ambient conditions was taken for $AlBO_3$, $FeBO_3$ and $InBO_3$, and powder x-ray diffraction data was taken for $ScBO_3$ to confirm the calcite-type structure of our samples which has been also confirmed by Raman scattering measurements (not shown).

HP experimental details.- HP angle-dispersive powder X-ray diffraction experiments were conducted at room temperature in Diamond (I15 beamline) and ALBA (MSPD beamline [21]) synchrotron light sources. Experiments on $AlBO_3$, $ScBO_3$, $FeBO_3$ and $InBO_3$ were carried out up to 31, 18, 31, and 32 GPa, respectively, with a monochromatic wavelength of 0.4246 Å. The samples were loaded in 150 µm diameter holes of 40 µm thick of inconel gaskets in modified Merrill-Bassett or membrane-type diamond-anvil cells (DACs) with diamond culet sizes of 450 µm. A 16:3:1 methanol-ethanol-water mixture was used as pressure-transmitting medium. The monochromatic X-ray beam was focused down to 20 × 20 µm using Kirkpatrick-Baez mirrors. A pinhole placed before the sample position was used as a cleanup aperture for filtering out the tail of the X-ray beam. The images were collected using a Mar350 image plate for $(Al,Sc)BO_3$ and a SX-165 CCD for $(Fe,In)BO_3$.

Pressure was measured by the ruby fluorescence method [22]. Preliminary data reduction was done using the Fit2D software [23]. The indexing and refinements of the powder diffraction patterns were performed using the FULLPROF [24] and POWDERCELL [25] program packages.

First-principles calculations.- Total-energy *ab initio* simulations have been performed within the density-functional theory (DFT) framework as implemented in the Vienna *ab initio* simulation package (VASP) (see Refs. 26 and 27 and references therein). The program performs *ab initio* structural calculations with the plane-wave pseudo-potential method. The set of plane waves employed extended up to a kinetic energy cutoff of 520 eV. Such a large cutoff was required to achieve highly converged results within the projector-augmented-wave (PAW) scheme [28]. The exchange-correlation energy was taken in the generalized gradient approximation (GGA) with the PBEsol prescription [29]. The GGA+U method is used for the case of $FeBO_3$ to account for the strong correlation between the electrons in the Fe d shell, on the basis of Dudarev's method [30]. In this method, the onsite Coulomb interaction U and the onsite exchange interaction J are treated together as $U_{eff} = U - J$. For our GGA+U calculations, we choose U_{eff} = 4 eV for the Fe atom, value used in a previous study on some metal-rich borides [31]. Our study shows that $FeBO_3$ is an antiferromagnetic material.

We used a dense Monkhorst-Pack [32] k-special point grid to perform accurate and well converged energies and forces calculations. At each selected volume, the structures were fully relaxed to their equilibrium configuration through the calculations of the forces on the atoms and the stress tensor, which means that we obtain the evolution with pressure of the internal and external parameters of the structure under study. It is useful to note that the theoretical pressure P(V), can be obtained within the *ab initio* DFT calculations at the same time that the E(V) data. The theoretical pressure, P, like other derivatives of the energy, is obtained from the diagonal stress tensor achieved after the structural relaxation [33].

3.- Experimental and theoretical high-pressure results

Table I collects the crystallographic information for the four rhombohedral calcite-type orthoborates under study from Rietveld refinements carried out at ambient conditions. Theoretical structural data of the orthoborates are also included in **Table I** and present a good agreement with our measurements.

Table I. Experimental (Exp.) and theoretical (Theor.) crystallographic parameters of the ABO_3 (A=Al,Fe,Sc,In) borates at ambient conditions. They are described with a rhombohedral R-3c space group (No. 167), where the A and B cations are located at the 6b (0,0,0) and 6a (0,0,0.25) Wyckoff positions, respectively. The oxygen is located at the 18e (x,0,0.25) Wyckoff position.

	a (Å)	c (Å)	O site: 18e	
$AlBO_3$	4.4638(3)	13.745(1)	x = 0.30907(6)	Exp. (Ref. 5)
	4.47765	13.72305	x = 0.30902	Theor.
$FeBO_3$	4.626(1)	14.493(6)	x = 0.2981(4)	Exp. (Ref. 7)
	4.6352	14.43033	x = 0.29847	Theor.
$ScBO_3$	4.754(1)	15.277(1)	x = 0.286(1)	Exp.
	4.76517	15.20694	x = 0.29036	Theor.
$InBO_3$	4.8180(4)	15.4290(3)	x = 0.3115(6)	Exp.
	4.8572	15.44305	x = 0.2846	Theor.

Under compression, X-ray powder diffraction patterns of borates do not show any significant change within the studied pressure range and could be indexed in the rhombohedral phase up to the maximum pressure of this study. **Figure 2** depicts the integrated intensities as a function of 2θ at selected pressures in $AlBO_3$ to show the quality of these data, which allow Rietveld structural analyses. On the other hand, crystal sizes of the $(Sc,Fe,In)BO_3$ powder samples are not uniform and, consequently, some texturing effects appear in the x-ray diffraction patterns. This unwanted effect entails that the relative intensities of the diffraction maxima are not accurate, avoiding full structural refinements for these three borates. Above 10 GPa, the diffraction peaks broaden gradually as a consequence of the loss of the quasi-hydrostatic conditions and the appearance of deviatoric stresses in the compressed samples. This is expected because of the use of the methanol-ethanol-water mixture as pressure transmitting medium [34,35].

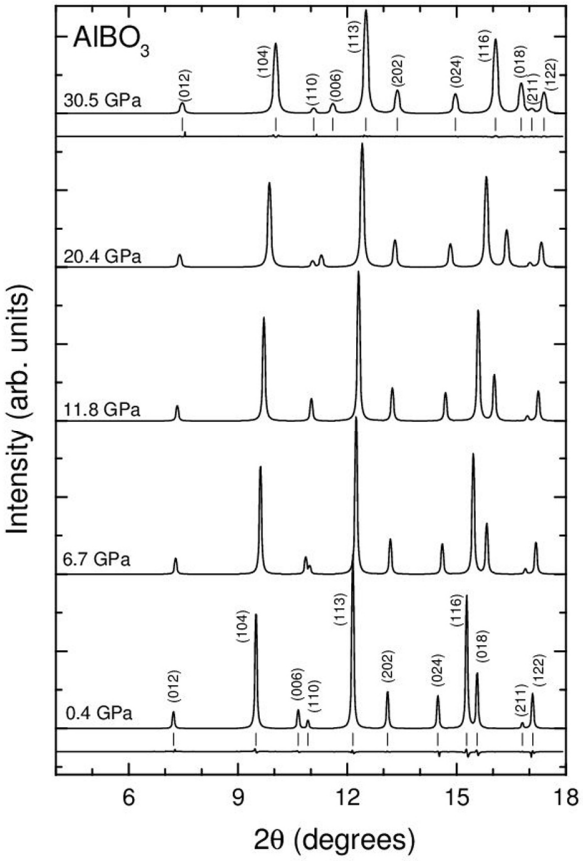

Figure 2.- Powder XRD patterns of $AlBO_3$ at five selected pressures. The calculated profiles and the residuals of the Rietveld refinements at 0.4 and 30.5 GPa are also represented. Vertical marks indicate the Bragg reflections of the rhombohedral R-3c structure at 0.4 and 30.5 GPa.

Rietveld refinements carried out on HP-XRD data for $AlBO_3$ show that the *x* atomic coordinate of the O atom up to 31 GPa was similar to that at ambient conditions within experimental uncertainty. This result agrees with the weak pressure dependence of this atomic parameter obtained from our theoretical calculations (according to simulations the x coordinate of $AlBO_3$ varies from 0.30902 at 0 GPa to 0.3128 at 30 GPa).

The pressure evolution of the unit-cell volumes of the four borates is plotted in **Fig. 3**, where we compare them with those obtained in our theoretical calculations. The pressure-volume curves were analyzed using a second-order Birch-Murnaghan (BM) equation of state (EOS) [36]. In the fitting of the experimental values, the zero-pressure volume (V_o), and the bulk modulus (B_o) are left as free parameters whilst the bulk modulus pressure derivative (B_o') is fixed to 4. In the case of the calculations the B_o' parameter is left free in the EOS fitting obtaining values for B_o' close to 4. The obtained values for V_o, B_o and B_o' are collected in **Table II**. Experimental values of the bulk modulus are in good agreement with those obtained from *ab-initio* calculations. The obtained experimental values for B_o decrease following the sequence "$AlBO_3$ > $ScBO_3$ > $InBO_3$". Special mention deserves the $FeBO_3$ dataset. A previous study by Gavriliuk *et al.* reported the EOS of the calcite-type phase of this compound up to 54 GPa using silicon organic liquid as pressure transmitting medium [37]. Their results are included in **Table II**. Their P-V data points present a large dispersion but an overall agreement with our results when our EOS fit is carried out in the range 0-30.5 GPa. However, above 10 GPa, our experimental data starts to deviate from the theoretical predicted P-V curve for reasons that are not obvious, showing a change in tendency with pressure that suggests that a better estimation for the EOS parameters is obtained when the fit is restricted to the range 0-10 GPa. For this reason, we have also obtained the EOS parameters for $FeBO_3$ using experimental data in the range 0-10 GPa and the results are included in **Table II**. In this case, the theoretical values B_o compare well with the experimental ones.

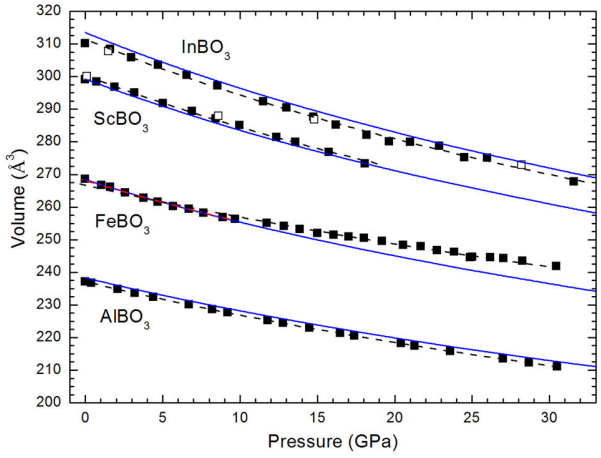

Figure 3.- Pressure dependence of the experimental (symbols) and theoretical (blue solid lines) unit-cell volumes of Al, Sc, Fe and In borates. Solid symbols refer to data taken in the upstroke and open symbols to data taken in the downstroke. Black dashed lines represent the fit with a BM EOS to experimental data in the whole pressure range. For the case of $FeBO_3$, the fit with a BM EOS to experimental data in the range 0-10 GPa is shown with a dash-dotted red line.

Table II. Experimentally determined and calculated EOS parameters for ABO_3 (*A*=Al, Fe, Sc, In) borates at ambient conditions. A BM EOS has been used for the fits. The pressure range used in the EOS fits is indicated in the table for the experimental data. In the case of $FeBO_3$, data from Ref. 35 is included for comparison purposes.

	V_o (Å^3)	B_o (GPa)	B_o'		**Pressure range (GPa)**
$AlBO_3$	237.15(1)	207.2(2)	4 (fixed)	Exp.	0-30.5
	238.28(1)	210.3(5)	4.24(3)	Theor.	
$FeBO_3$	266.7(3)	250(5)	4 (fixed)	Exp.	0-30.5
	268.1(2)	188(5)	4 (fixed)	Exp.	0-9.7
	266.5	255(25)	5.0(1.2)	Exp.	0-54 (Ref. 37)
	268.38(3)	181.6(6)	4.21(5)	Theor.	
$ScBO_3$	300.3(4)	166(4)	4 (fixed)	Exp.	0-18.1
	299.19(4)	167.7(6)	3.93(4)	Theor.	
$InBO_3$	311.5(5)	158(3)	4 (fixed)	Exp.	0-31.6
	313.46(3)	160.3(5)	3.88(3)	Theor.	

Figure 4 illustrates the evolution of the lattice parameters *a* and *c* with increasing pressure which evidence that their contraction is rather anisotropic; *i.e.* according to our experiments, the compressibilities of the *a* axes are considerably smaller than those of the corresponding *c* axes. **Table III** reports the experimental and theoretical axial compressibilities for *a* and *c* axes at room pressure, defined as $\kappa_x = \frac{-1}{x}\frac{\partial x}{\partial P}$ and obtained by fitting of a Murnaghan EOS [38]. The theoretical values of κ_a and κ_c are in relatively good agreement with the experimental values and in all of the cases κ_c is greater than κ_a ($\kappa_c \sim 3\cdot\kappa_a$). This is due to the fact that the B – O bonds are less compressible than the *A* – O bonds and, as we will see below, to the tendency of the *AB* cation subarray to adopt a CsCl-like structure. Taking into account our calculations we have obtained that the interatomic *A* – O distances (*A* = Al/Sc/Fe/In) have shortened 1.6/1.9/1.8/2.0% between room pressure and 10 GPa, whereas the B – O distance only varies 0.6/0.7/0.7/0.8% in the same pressure range. Moreover, non-hydrostaticity likely produces a slight change in the slope of the *c*/*a* axes ratio of these borates at the hydrostaticity limit, which indicates that the compression ratio between [AO_6] octahedra and [BO_3] triangles is affected by deviatoric stresses.

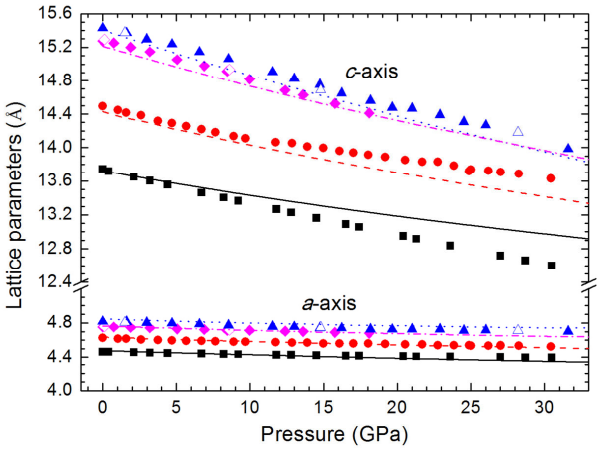

Figure 4.- Pressure dependence of the lattice parameters. Black squares, red circles, magenta diamonds and blue triangles represent experimental data for Al, Fe, Sc and In borates, respectively. Solid (open) symbols refer to data taken in the upstroke (downstroke). Solid black line, dashed red line, dash-dotted magenta line and dotted blue line represent calculations for Al, Fe, Sc and In borates, respectively.

Table III. Experimentally determined and calculated axial compressibilities κ_a and κ_c (10^{-3} GPa^{-1}) for ABO_3 (*A*=Al, Fe, Sc, In) borates at ambient conditions.

	κ_a	κ_c		**Pressure range (GPa)**
$AlBO_3$	0.98(4)	3.05(2)	Exp.	0-30.5
$AlBO_3$	1.19(1)	2.35(1)	Theor.	
$FeBO_3$	0.87(3)	2.32(4)	Exp.	0-30.5
$FeBO_3$	1.2(1)	3.8(1)	Exp.	0-9.7
$FeBO_3$	1.26(1)	2.99(2)	Theor.	
$ScBO_3$	1.13(3)	3.6(3)	Exp.	0-18.1
ScBO3	1.30(2)	3.40(3)	Theor.	
$InBO_3$	1.6(2)	3.49(5)	Exp.	0-31.6
$InBO_3$	1.38(3)	3.75(3)	Theor.	

The present HP experimental work on a series of ABO_3 (*A* = Al, Sc, Fe, In) borates makes possible to analyze the compressibility behaviour of these compounds depending on the nature of the trivalent *A* metal. Anderson and Anderson [39] noted that, to a first approximation, in many oxides with the same crystal structure the relationship B_oV_o = constant is held. Using our results we can explore the applicability of this behaviour to rhombohedral orthoborates. Thus, we see that reciprocal volume and bulk modulus both decrease with increasing radii of the *A* metal ion (inferred from **Table II**) and that the volume-compressibility relationship for this set of samples does indeed approximate to the B_oV_o constant conjecture as shown in **Fig. 5**. It is also important to emphasize that the bulk compressibility of these compounds is governed by that of the [AO_6] octahedra, given the high incompressibility of the [BO_3] units. In this respect we have to note that the octahedral compressibility in different compounds apparently decreases with the connectivity of the [AO_6] octahedra; for instance, in compounds with [AlO_6] octahedra the compressibility of this unit decreases from corundum Al_2O_3 (sharing faces, B_{Oh} = 276(3) GPa, B_{Oh}' fixed to 4) [40], through spinel $MgAl_2O_4$ (sharing edges, B_{Oh} = 239 GPa, B_{Oh}' = 4.59) [41], to $AlBO_3$ (sharing corners, B_{Oh} = 182.8(3) GPa, B_{Oh}' fixed to 4). It is also worthy to mention that, in spite of having 6 equal *A* – O distances in the [AO_6] units at room conditions, our calculations show that the octahedra of the calcite structure are slightly distorted. In particular, they show two different O – *A* – O angles with values 88.4º/91.7º, 87.9º/92.1º, 88.4º/91.6º/ and 88.4º/91.6º for Al, Sc, Fe and In borates, respectively. According to calculations, these octahedra become more symmetric with increasing pressure (regular octahedra at 68.9/29.5/28.3/16.0 GPa for Al, Fe, Sc and In borates, respectively). Surprisingly, our calculations show that the calcite structure in $ScBO_3$ becomes mechanically unstable at a pressure 1.2 GPa higher than that when [ScO_6] units adopt a regular octahedral configuration. For the other three calcite-type borates, simulations predict that the mechanical instability occurs at pressures well above those where regular [AO_6] octahedra form. The influence of distortions and tilting of octahedra on crystalline stability is well known for other ABO3 compounds like perovskites [42]. The observed mechanical instability of borates could likewise be related to electronic instabilities due to orbital degeneracies associated to octahedral regularity, but this fact remains unclear. A detailed analysis of these effects is beyond the scope of the present work.

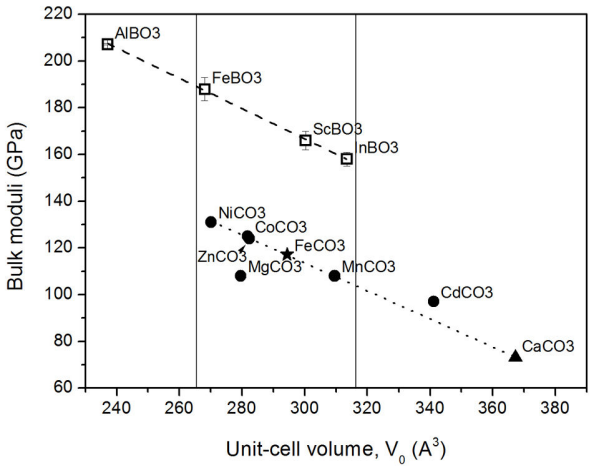

Figure 5.- Bulk modulus – Unit cell volume relationships for rhombohedral calcite-type borates and carbonates. Data for (Mg,Mn,Co,Ni,Zn,Cd)CO_3 carbonates are from [51] and are represented as solid circles, calcite $CaCO_3$ from [43] (solid triangle), siderite $FeCO_3$ from [52] (solid star), and borates from this study (empty squares). The B_oV_o product is constant for borates. The slope of the B_o - V_o lineal fittings for both borates and carbonates is comparable (dashed and dotted lines, respectively).

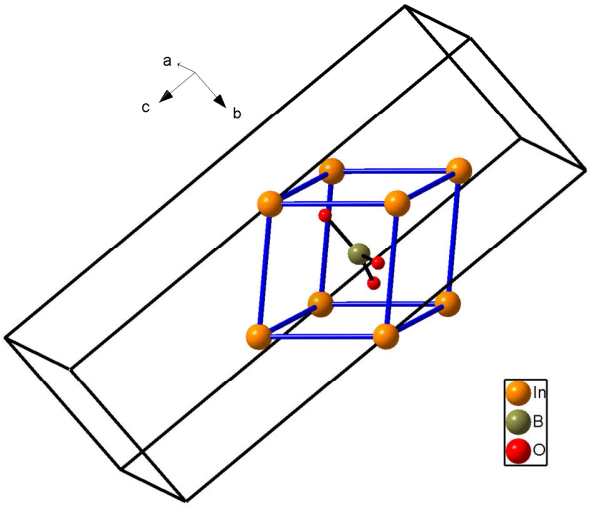

Figure 6.- Underlying CsCl-type structure of the InB subarray in $InBO_3$ (angle ∠In-In-In = 79º at room conditions).

Structural changes observed in ABO_3 borates under compression can be rationalized if one analyses of the second coordination sphere of the metallic atoms, the cation *A*B subarray. While [AO_6] units smoothly transform into perfect octahedra as pressure increases, the decrease of the hexagonal distortion of the lattice, which is described by the approach of the $t = 2a\sqrt{2}/c$ parameter to 1 [43], produces that the *A*B substructure, above described as a distorted NaCl-type net at room pressure, progressively evolves towards a CsCl-type structure (see **Fig. 6**). This feature becomes evident, for instance, looking at the two angles of the underlying distorted NaCl-type and CsCl-type cubes of any of the four orthoborates. For instance, in $InBO_3$, the first angle changes from 76.4º at room pressure to 74.5º at 31 GPa, distancing from the ideal angle (90º) of a cubic NaCl-type structure with increasing pressure. The second angle, on the other hand, changes from 79.0º to 82.1º in the same pressure range, gradually approaching to the ideal angle (90º) of the cubic CsCl-type configuration. This observation is consistent with the behaviour of many *AX* binary compounds which follow the rocksalt to cesium chloride structural sequence under pressure. Intermediate structures between the rocksalt and the cesium chloride are found in cation subarrays of oxides [44, 45] with coordination numbers ranging from 6 to 8.

In fact, the cation array in orthoborates can be seen as a strong distortion of the atomic arrangement of the intermetallic compound FeB or vice versa (compare both structures depicted in **Fig 7a and 7d**). The displacement of the z coordinate of the Fe (z ~0.12) and B (z ~0.64) atoms in the FeB structure to positions defined by z = ¼ and ¾, respectively, would entail the formation of an atomic arrangement comparable to that of the FeB subarray in $FeBO_3$ (see intermediate structures in **Figs. 7b and 7c**) . Therefore, iron boride and the cation subarray of iron borate are forming intimately related structures despite the fact that the latter is embedded in an oxygen matrix. This is in good agreement with the observation of cation substructures of oxides as being the leading parts of the structure which is distorted by oxygens. In this sense, oxides can be understood as metal frameworks stuffed with oxygens that exert a chemical pressure over the metal framework thus distorting it [13-16,44,46].

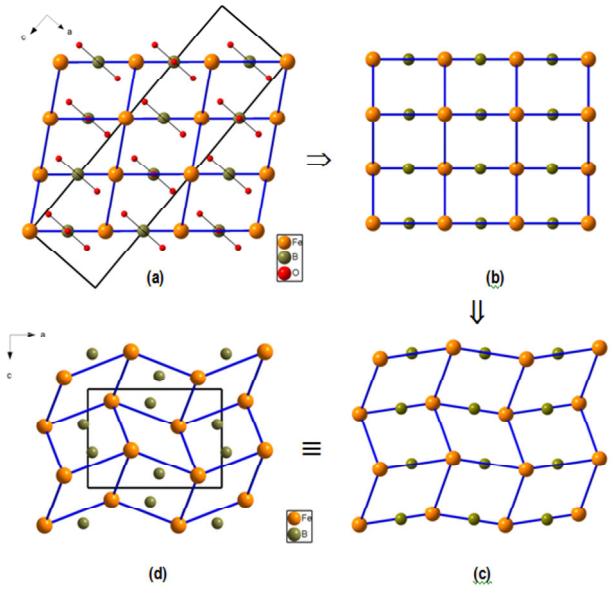

Figure 7.- (a) Calcite-type structure of $FeBO_3$ viewed along *b*. Fe – Fe contacts and the unit-cell edges are drawn as solid blue and solid black lines, respectively. The distorted trigonal prisms [Fe_6] share faces in the *b* direction. (d) The structure of the FeB alloy, projected on the same plane, to show its similarity with the cation subarray of $FeBO_3$. (b) and (c) Potential intermediate structures between the actual cation network of calcite orthoborates and the FeB alloy.

A comparison of the studied orthoborates with their isostructural and isoelectronic carbonates ($MgCO_3$/$AlBO_3$, $CaCO_3$/$ScBO_3$, $MnCO_3$/$FeBO_3$, $CdCO_3$/$InBO_3$ couples) could be very instructive. According to the ionic bonding approximation, and taking into account that $[BO_3]^{3-}$ are more charged than $[CO_3]^{2-}$ units, orthoborates should be more incompressible and stable than carbonates and could provide a larger P-T range for structural studies; i.e. orthoborates are stable calcite-type carbonate analogues. Both, high stability and higher bulk moduli are confirmed experimentally in this work. In fact, no structural phase transitions exist in scandium and indium borates in the range 0-18 and 0-32 GPa, respectively, whereas their carbonate counterparts $CaCO_3$ calcite and $CdCO_3$ otavite transform into monoclinic calcite II and aragonite (NiAs-type in *AB* subarray) phases at 1.6 GPa and 17 GPa (and 1000 K temperature), respectively [47,48]. $MgCO_3$ magnesite is very stable and only converts into a new phase at 100 GPa [49] whereas $AlBO_3$ is predicted to be mechanically stable up to 106.5 GPa [42]. In the fourth couple, $MnCO_3$ rhodochrosite transforms at 50 GPa after laser heating [50] and $FeBO_3$ at 53 GPa at room temperature [37]. Bulk and axial compressibilities, on the other hand, are clearly smaller in the case of orthoborates with the exception of κ_a for the pair $InBO_3$ and $CdCO_3$. A comparison of our compressibility values and the results on carbonates [43,51] is collected in **Table IV**. Linear B_o – V_o fittings depicted in **Fig. 5**, give the following relationships: B_o(GPa) = 361(3) – 0.65(1)·V_o for borates and B_o(GPa) = 294(2) – 0.600(5)·V_o for carbonates (not considering $MgCO_3$ and $CdCO_3$). Taking into account the calcite-type phase overlapping of both families (indicated within vertical bars in **Fig. 5**), which occurs for ionic *A* radii between 80 and 97 pm, it can be inferred that In, Sc, Ti and Fe borates are potential good analogues to model carbonates such as siderite ($FeCO_3$) of great interest in Earth sciences. This potential analogy is corroborated by the fact that these borates present similar values for the hexagonal distortion at room conditions than carbonates. Nevertheless, from the equations aforementioned, the difference in bulk moduli between both families of calcite-type compounds for similar unit-cell volumes at room pressure are in the range 55-60 GPa.

Table IV. Experimental axial compressibilities κ_a and κ_c(10^{-3} GPa^{-1}), bulk modulus B_o(GPa) and hexagonal distortion (t = $2a\sqrt{2}/c$) at room pressure for our four borates and the isoelectronic ACO_3 (A=Mg, Ca, Mn, Cd) carbonates.

	κ_a	κ_c	B_o	Hexagonal distortion	Reference
$AlBO_3$	0.98(4)	3.05(2)	207.2(2)	0.91855	This work
$MgCO_3$	2.13(7)	4.03(5)	107(1)	0.87301	51
$FeBO_3$	1.2(1)	3.8(1)	188(5)	0.90280	This work
$MnCO_3$	1.76(4)	4.84(6)	108(1)	0.86106	51
$ScBO_3$	1.13(3)	3.6(3)	166(4)	0.88023	This work
$CaCO_3$	2.4(3) 2.62(2)	9.4(9) 7.94(7)	67(2) 73.5(3)	0.82792	51 43
$InBO_3$	1.6(2)	3.49(5)	158(3)	0.88323	This work
$CdCO_3$	1.34(5)	6.36(7)	98(1)	0.85435	51

4.- Concluding remarks

In this paper we report an experimental and theoretical study of the compressibility and structural stability of Al, Fe, Sc and In orthoborates by angle-dispersive x-ray diffraction measurements in synchrotron radiation sources and *ab initio* total-energy (DFT-GGA-PBEsol) calculations. Our results show that the initial R-3c calcite-type phase remains stable within the whole pressure

range of this study (up to 31, 31, 18 and 32 GPa, respectively). Experimental and calculated static geometries, bulk moduli and axial compressibilities are in good agreement. The anisotropic contraction of the lattice constants ($\kappa_c \sim 3 \cdot \kappa_a$) produces a significant change in the second coordination sphere of cations, as inferred from the analysis of the *A*B substructure, evolving towards a CsCl-type structure with increasing pressure. This different axial compressibility in borates is a consequence of the distribution of the [BO_3] and [AO_6] polyhedra in the unit-cell and is clearly dominated by the compressibility of the [AO_6] octahedral site which, in turn, depends on the size of the trivalent *A* cation. Our results evidence that the relationship B_oV_o = constant is hold for borates.

A comparison with the isostructural carbonate minerals shows that borates are more incompressible and stable. These two families of calcite-type chemical analogues present an interval of similar zero-pressure unitcell volumes and c/a axes ratio, but about 60 GPa difference in their bulk moduli. These results suggest that borates could model structural aspects of relevant Earth carbonates.

AUTHOR INFORMATION

Corresponding Author

* Dr. David Santamaria-Perez: dsantamaria@quim.ucm.es

Present Addresses

♣ Earth Sciences Dpt., University College London, UK

Author Contributions

The manuscript was written through contributions of all authors.

ACKNOWLEDGMENT

This study was supported by the Spanish government MEC under Grants No: MAT2010-21270-C04-01/03/04 and CTQ2009-14596-C02-01, by MALTA Consolider Ingenio 2010 Project (CSD2007-00045), by Generalitat Valenciana (GVA-ACOMP-2013-1012), and by the Vicerrectorado de Investigación y Desarrollo of the Universidad Politécnica de Valencia (UPV2011-0914 PAID-05-11 and UPV2011-0966 PAID-06-11). We thanks ALBA and Diamond synchrotrons for providing beamtime for the XRD experiments. A.M. and P.R-H. acknowledge computing time provided by Red Española de Supercomputación (RES) and MALTA-Cluster. J.A.S. and B. G.-D. acknowledge Juan de la Cierva fellowship and FPI programs for financial support. We want also acknowledge J.J. Capponi and R. Diehl for supplying us single crystals of $AlBO_3$ and $FeBO_3$, respectively.

REFERENCES

[1] R. D. Shannon, Acta Cryst. A (1976) **32**, 751-767.

[2] E. M. Levin, R. S. Roth, J. B. Martin, Amer. Mineral. (1961) **46**, 1030-1055.

[3] V. A. Blatov, Y.A. Zakutkin, Z. Kristallogr. (2002) **217**, 464-473.

[4] H.E. Suess, Rev. Modern Phys. (1956) **28**, 53-74.

[5] A. Vegas, F. H. Cano, S. Garcia-Blanco, Acta Cryst. B (1977) **33**, 3607-3609.

[6] A. Biedl, Amer. Mineral.(1966) **51**, 521-524.

[7] R. Diehl, Solid State Comm. (1975) **17**, 743-745.

[8] J. R. Cox, D. A. Kezzler, Acta Cryst. C (1994) **50**, 1857-1859.

[9] F.J. Avella, O.J. Sovers, C.S. Wiggins, J. Electrochem. Soc. (1967) 114, 613-616.

[10] S.T. Lai, B.H.T. Chai, M. Long, R.C. Morris, J. Quantum Elect. (1986) **22**, 1931-1933.

[11] M. Balcerzyk, Z. Gontarz, M. Moszynski, M. Kapusta, J. Lumin. (2000) **87**, 963-966.

[12] M.P. Petrov, A.R. Paugurt, G.A. Smolenskii, Phys. Lett. A (1971) **36,** 44-45.

[13] A. Vegas, M. Jansen, Acta Cryst. B (2002) **58**, 38-51.

[14] D. Santamaria-Perez, A. Vegas, F. Liebau, Struct. Bond. (2005) **118**, 121-177.

[15] A. Vegas, M. Mattesini, Acta Cryst. B (2010) **66**, 338-344.

[16] D. Santamaria-Perez, R. Chulia-Jordan, High Press. Res. (2012) **32**, 81-88.

[17] A.J. Skinner, J.P. LaFemina, H.J.F. Jansen, Amer. Mineral. (1994) **79**, 205-214.

[18] J.J. Capponi, J. Chenavas, J.C. Joubert, Bull. Soc. Franç. Mineral. Crystallogr. (1972) **95**, 412-417.

[19] I. Bernal, C.W. Struck and J.G. White, Acta Cryst. (1963) **16**, 849-850.

[20] J.P. Chaminade, A. Garcia, M. Pouchard, C. Fouassier, B. Jacquier, D. Perret-Gallix, L. Gonzalez-Mestres, J. Cryst. Growth (1990) **99**, 799-804.

[21] M. Knapp, I. Peral, M. Nikitina, M. Quispe, S. Ferrer, Z. Kristallogr. Proc. (2011) **1**, 137-142.

[22] H. K. Mao, J. Xu, P. M. Bell, J. Geophys. Res.-Solid Earth and Planets (1986) **91**, 4673-4676.

[23] A. P. Hammersley, S. O. Svensson, M. Hanfland, A. N. Fitch, D. Hausermann, High Press. Res. (1996) **14**, 235-248.

[24] J. Rodriguez-Carvajal, Physica B (1993) **192**, 55-69.

[25] W. Kraus, G. Nolze, J. Appl. Cryst. (1996) **29**, 301-303.

[26] G. Kresse, J. Furthmuller, Phys. Rev. B (1996) **54**, 11169-11186.

[27] G. Kresse, D. Joubert, Phys. Rev. B (1999) **59**, 1758-1775.

[28] P.E. Blöchl, Phys. Rev. B (1994) **50**, 17953-17979.

[29] J. P. Perdew, A. Ruzsinszky, G. I. Csonka, O. A. Vydrov, G. E. Scuseria, L. A. Constantin, X. Zhou, K. Burke, Phys. Rev. Lett.(2008) **100**, 136406.

[30] S.L. Dudarev, G.A. Botton, S.Y. Savrasov, C.J. Humphreys, A.P. Sutton, Phys. Rev. B (1998) **57**, 1505-1509.

[31] I.M. Ndassa, M. Guilleβen, B.P.T. Fokwa, Solid State Sci. (2013) **17**, 14-20.

[32] H.J. Monkhorst, J.D. Pack, Phys. Rev. B (1976) **13**, 5188-5192.

[33] A. Mujica, A. Rubio, A. Muñoz, A. Rev. Mod. Phys. (2003) **75**, 863-912.

[34] D. Errandonea, Y. Meng, M. Somayazulu, D. Häusermann, Physica B (2005) **355**, 116-125.

[35] S. Klotz, J.C. Chervin, P. Munsch, G. Le Marchand, J. Phys. D: Appl. Phys. (2009) **42**, 075413.

[36] F. Birch, J. Geophys. Res. (1978) **83**, 1257.

[37] A. G. Gavriliuk, I. A. Trojan, R. Boehler, M. Eremets, A. Zerr, I. S. Lyubutin, V. A. Sarkisyan, JEPT Lett. (2002) **75**, 23-25.

[38] M. D. Frogley, J. L. Sly, and D. J. Dunstan, Phys. Rev. B (1998) **58**, 12579.

[39] D.L. Anderson, O.L. Anderson, J. Geophys. Res. (1970) **75**, 3494-3500.

[40] J.R. Smyth, S.D. Jacobsen, R.M. Hazen, Rev. Mineral. (2000) **40**, 1-23.

[41] U.D. Wdowik, K. Parlinski, A. Siegel, J. Phys. Chem. Solids (2006) **67**, 1477-1483.

[42] J.M. Rondinelli, S.J. May, J.W. Freeland, MRS Bull. (2012) **37**, 261-270.

[43] S.A.T. Redfern, R.J. Angel, Contrib. Mineral Petrol. (1999) **134**, 102-106.

[44] A. Vegas, Crystallogr. Rev. (2000) **7**, 189-283.

[45] D. Santamaria-Perez, L. Gracia, G. Garbarino, A. Beltran, R. Chulia-Jordan, O. Gomis, D. Errandonea, Ch. Ferrer-Roca, D. Martinez-Garcia, A. Segura, Phys. Rev. B (2011) **84**, 054102.

[46] L.A. Martinez-Cruz, A. Ramos-Gallardo, A. Vegas, J. Solid State Chem. (1994) **110**, 397–398.

[47] P.W. Bridgman, Amer. J. Sci. (1939) **237**, 7-18.

[48] L.G. Liu, C.C. Lin, Amer. Mineral. (1997) **82**, 5-6.

[49] M. Isshiki, T. Irifune, K. Hirose, S. Ono, Y. Ohishi, T. Watanuki, E. Nishihori, M. Takadda, M. Sakata, Nature (2004) **427**, 60-63.

[50] S. Ono, Mineral. Mag. (2007) **71**, 105-111.

[51] J. Zhang, R.J. Reeder, Amer. Mineral. (1999) **84**, 861-870.

[52] J. Zhang, I. Martinez, F. Guyot, R.J. Reeder, Amer. Mineral. (1998) **83**, 280-287.